GSICS Global Space-based Inter-Calibration System

Quarterly

Newsletter Spring 2021 Issue

doi: 10.25923/m6pq-w122
Vol. 15 No 1, 2021
Editor: Manik Bali, ESSIC/UMD

Articles

News in This Quarter

Announcements

GSICS Related Publications

Part-II: GSICS Annual State of Observing System

Status of GSICS monitored instruments

By Mitch Goldberg (NOAA) and Manik Bali (ESSIC/UMD)

In this (Part-II) of the special issue on the GSICS State of Observing System we provide the most updated assessment of the satellites monitored by GSICS member agencies. These assessments are determined by comparing satellites with robust GSICS designated in-orbit references.
Articles in this issue contributed by GSICS members, aim to reveal the most updated status of a range of satellite instruments monitored by them.

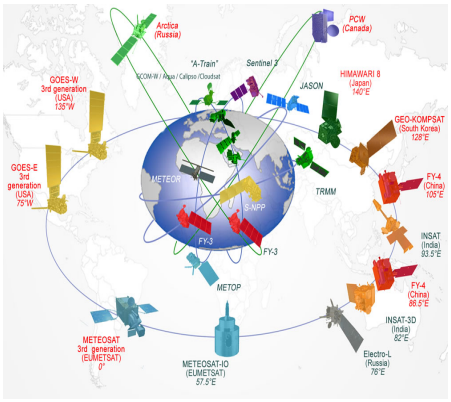

Image Curtsey WMO: Shows Satellites of Space observing System. https://public.wmo.int/en/programmes/wmo-space-programme

A quick review of the GSICS Processing Research Centers (https://gsics.wmo.int/en/product-services-and-technical-information) maintained by GSICS members reveal that in the past year GSICS members kept moving forward and are now monitoring instruments on over 26 satellites and share the biases in real time. The monitored instruments belong to the families of GOES, Meteosat, Metop-HIRS, MSU-MR, IKFS, MSU-GS, FY, GK-2A, Himawari and INSAT. Instruments on-board these platforms take measurements in Ultraviolet, Visible, Infrared and Microwave wavelengths. GSICS members also continued to deliver these biases as GSICS products via the GSICS product catalog.
NOAA added new monitoring products for GOES-16/17 by comparing with CrIS as well as IASI-B/C thereby providing a diurnal validation of the GOES performance. Wu et al. in the following article report that there are no noticeable changes in GOES -16/17 biases in 2020.

Figure 1 on the next page shows the similarity between the mean bias for MSG-1/2/3/4 and Himawari-8 over their spectrum for the year 2020. The third article by Hewison shows that the MSG series retained low bias drifts. Earlier Hu et al. 2021 have shown FY-4A Agri biases range -3.8K -0.1265 K in the IR spectrum when IASI-B is used as a reference. The fourth article by Rublev et al. shows the progress they have made in maintaining their in-orbit IR and Microwave instruments. The next two articles give details on the performance of GK-2A and Himawari-8.

IASI-B/C are GSICS references, and their status is discussed by Laura Le Barbier and Clémence Pierangelo (CNES).

The concluding article by Tom Stone presents high spectral resolution Solar Datasets constructed by Odele Coddington that span the 202 nm -2730 nm range with a uncertainty better than 1.3%. Tom proposes this data set as GSICS Reference Solar.

doi: 10.25923/m6pq-w122

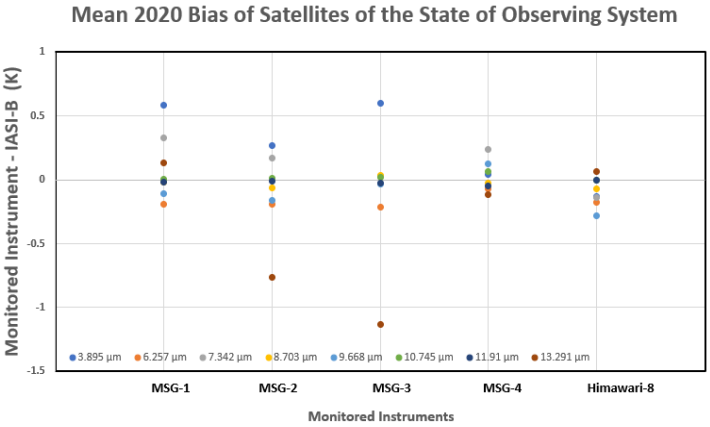

Figure 1: Above shows mean bias taken from GSICS Product Catalog Shows biases of MSG-1/2/3/4 and Himawari-8 for the year 2020. Similarity between biases of different instrument demonstrate the robustness of the underlying instruments and algorithms.

Conclusion

In summary GSICS members continue to monitor their satellites by computing biases and offsets relative to GSICS references. Further, as highlighted in the recent GSICS Annual meeting 2021, member agencies have made significant advances in using the GSICS generated biases to re-calibrate the measurements and produce a stable time series.

Member agencies also envisage a promising **outlook for the coming year** wherein measurements quality and uptime of satellite data are maintained within design specifications.

GSICS references, IASI-B/C, VIIRS/CrIS-SNPP/NOAA-20 have continued to deliver reference scale measurements well beyond design specifications thus maintaining the GSICS inter-calibration framework, and new Solar Reference data sets have added a new dimension to improving UV-VIS-NIR calibration.

References

Hu et al. 2021, CMA Agency Report, GSICS Annual Meeting. http://gsics.atmos.umd.edu/pub/Development/Annual2021/1f_GSICS%20Agency%20Report_2021_CMA.pdf

NOAA 2020 GSICS Annual Report for GOES-16/17 ABI

By Xiangqian Wu, Fangfang Yu, Hye Lim Yoo, NOAA

NOAA monitors its GEO constellation consisting of the GOES-R series in VNIR and IR channels. Details of the biases are at https://www.star.nesdis.noaa.gov/GOESCal/index.php.
Tables 1 and 2 give the tabulated mean and standard deviation of biases in 2020.

Summary of Instrument Biases

- NOAA monitors the visible and near infrared channels of ABI on GOES-16/17 by comparing them with VIIRS on NOAA-20, using the ray matching method.
- NOAA also monitor this bias by comparing with VIIRS on S-NPP. The results are not reported here because of known differences between the two VIIRS.
- NOAA monitored IR channels of ABI on GOES-16/17 by comparing with IASI on METOP-A/B/C and with CrIS on S-NPP and NOAA-20. IASI –A results are not reported here since it is nearing its end-of-life.

Table 1: Mean and standard deviation of differences (GEO – LEO, % @ 100%) of GOES-16/17 ABI visible and near infrared channels in 2020, as compared with NOAA-20 VIIRS using the ray matching method.

	Channel 1 (0.47 µm)	Channel 1 (0.64 µm)	Channel 3 (0.86 µm)	Channel 4 (1.38 µm)	Channel 5 (1.61 µm)	Channel 6 (2.23 µm)
GOES-16	7.8±1.1	2.2±1.0	4.0±1.3	-0.2±1.9	3.1±4.0	1.6±1.4

Table 2: Mean and standard deviation of bias (mK @ 300 K) of GOES-16/17 ABI IR channels in 2020, as compared with IASI on METOP-B/C and CrIS on S-NPP and NOAA-20 at nighttime. GOES-17 results are for the period on each day when the Focal Plane Module (FPM) temperature is stable.

		Channel 7 (3.9 µm)	Channel 8 (6.2 µm)	Channel 9 (6.9 µm)	Channel 10 (7.2 µm)	Channel 11 (8.5 µm)	Channel 12 (9.6 µm)	Channel 13 (10.3 µm)	Channel 14 (11.2 µm)	Channel 15 (12.3 µm)	Channel 16 (13.3 µm)
GOES-16	IASI-B	-3±11	-31±3	-52±6	-29±7	-50±13	-70±10	-47±17	7±17	3±20	-140±18
	IASI-C	2±13	-29±3	-51±3	-30±7	-43±13	-42±10	-35±17	21±18	19±19	-119±20
	S CrIS	-	-	-38±5	-11±8	-	-11±8	-22±12	29±12	33±14	-104±12
	N CrIS	-	-	-28±5	3±7	-	9±8	41±13	95±13	92±16	-70±12
GOES-17	IASI-B	-36±14	-26±10	31±5	-6±14	-1±15	-89±14	-58±18	-50±20	59±22	326±20
	IASI-C	-26±13	-24±10	32±5	-8±12	2±13	-64±12	-49±15	-40±18	73±18	346±19
	S CrIS	-	-	55±6	12±12	-	-41±11	-39±10	-34±13	79±14	358±16
	N CrIS	-	-	67±6	31±10	-	-15±11	31±10	38±15	144±15	394±16

- GSICS Corrections have been generated and monitored but not applied.
- CrIS does not cover the full spectrum of Channel 7 (3.9 µm), 8 (6.2 µm), and 11 (8.5 µm). The missing spectral radiances can be omitted or estimated ("gap filling") for comparison. NOAA will release these comparisons after evaluating which method is better to

doi: 10.25923/m6pq-w122

monitor the instrument performance stability.

- GOES-17 operates at a higher temperature than designed, which alters its spectral response function (SRF). The updated SRF has not been implemented, therefore the biases are larger than they should be for some channels, particularly for the 13.3 µm channel.
- There is no noticeable change in bias in 2020 from past years.

Calibration Events in 2020

- Nothing major. https://www.star.nesdis.noaa.gov/GOESCal/goes_SatelliteAnomalies.php has details of minor events.

Outlook for the coming year

GOES-T is scheduled to launch on 7 December 2021. Post-launch tests will be executed in an expedited manner to conclude by June 2022. Impacts of this launch on GOES constellation and operation are unknown at this point.

EUMETSAT 2020 GSICS Annual Report for Meteosat/SEVIRI

By Tim Hewison, EUMETSAT

EUMETSAT monitors its GEO constellation consisting of the Meteosat series in VIS and IR channels.

Detailed time variation of the biases is available at the EUMETSAT GPRC. Below are the tabulated mean biases over 2020 (and mean rate of calibration drift over mission lifetime for VIS/NIR channels).

Summary of Instrument Biases

- GSICS DCC results still in demonstration phase – may include biases with respect to VIIRS.
- Meteosat-9 operated in Rapid Scan Service during most of this period, which increases the IR bias uncertainties Meteosat-10/SEVIRI IR13.4 channel now out of spec due to ice contamination.
- GSICS corrections can mitigate the bias and homogenize SEVIRI models.

EUMETSAT monitored IR channels of SEVIRI on Meteosat-8/9/10 IR by comparing with IASI on Metop-A/B/C. Since IASI –A is nearing end of life only IASI-B/C are considered for GSICS style monitoring to assess

2020 Meteosat/SEVIRI IR Channels Calibration Summary (*w.r.t. Metop-B/IASI*)

SEVIRI Channel Name		VIS0.6	VIS0.8	NIR1.6	HRV	Units
Meteosat-8	Mean Bias (DCC-SSCC)	+14.0 ± 2.3				%
	Annual Drift (All)	-0.58 ± 0.01	-0.55 ± 0.01	-0.04 ± 0.02	-0.54 ± 0.02	%/yr
Meteosat-9	Annual Drift (All)	-0.57 ± 0.01	-0.51 ± 0.01	-0.01 ± 0.02	-0.53 ± 0.02	%/yr
Meteosat-10	Annual Drift (All)	-0.79 ± 0.02	-0.72 ± 0.02	-0.05 ± 0.06	-0.80 ± 0.06	%/yr
Meteosat-11	Mean Bias (DCC-SSCC)	+10.47 ± 1.6				%
	Annual Drift (All)	-0.43 ± 0.03	-0.38 ± 0.12	-0.14 ± 0.23	-0.41 ± 0.21	%/yr

2020 Meteosat/SEVIRI VIS/NIR Channels Calibration Summary

SEVIRI Channel Name		IR3.9	IR6.2	IR7.3	IR8.7	IR9.7	IR10.8	IR12.0	IR13.4	Units
Meteosat-8	Standard Radiance as Tb	284	236	255	284	261	286	285	267	K
	Mean Bias and Std Dev	+0.58 ±0.03	-0.19 ±0.08	+0.33 ±0.10	-0.02 ±0.06	-0.11 ±0.10	+0.01 ±0.04	-0.02 ±0.04	+0.14 ±0.09	K
	Mean Drift Rate of Bias	-0.08	-0.12	-0.27	-0.08	-0.25	-0.09	-0.09	-0.26	K/yr
Meteosat-9	Mean Bias and Std Dev	+0.27 ±0.07	-0.19 ±0.06	+0.17 ±0.05	-0.07 ±0.04	-0.16 ±0.05	+0.01 ±0.02	-0.01 ±0.01	-0.76 ±0.30	K
	Mean Drift Rate of Bias	+0.18	-0.11	-0.07	+0.03	-0.05	+0.01	-0.01	+0.42	K/yr
Meteosat-10	Mean Bias and Std Dev	+0.60 ±0.03	-0.21 ±0.04	+0.03 ±0.06	+0.03 ±0.08	-0.03 ±0.11	+0.02 ±0.06	-0.02 ±0.04	-1.14 ±0.09	K
	Mean Drift Rate of Bias	-0.03	-0.02	-0.06	-0.04	-0.04	-0.07	-0.03	-0.25	K/yr
Meteosat-11	Mean Bias and Std Dev	+0.59 ±0.03	-0.18 ±0.09	+0.35 ±0.09	-0.02 ±0.05	-0.12 ±0.08	+0.01 ±0.04	-0.02 ±0.04	+0.22 ±0.07	K
	Mean Drift Rate of Bias	-0.07	-0.19	-0.14	-0.03	-0.14	-0.06	-0.06	-0.20	K/yr

biases. It is determined that these instruments retained biases as in the past year and as reported in the Calibration Report to CGMS-46.

Major Calibration Relevant Events in 2020

2020-01-27/02-13 Meteosat-9 Decontamination 2020-01-13/01-17 Meteosat-11 Decontamination

Outlook for the coming year

The Meteosat constellation components are expected to continue operating in the current configurations throughout most of 2021. Beyond that, Meteosat-8 will end operations on 2022-06-30. End of life technical tests will then be conducted until 2021-10-05, when it will be passivated and re-orbited. These tests include several of interest to GSICS partners, including a decontamination and performing rapid scans of the Moon over an extended period and with modified gain settings to acquire unsaturated IR lunar images.

doi: 10.25923/m6pq-w122

On-orbit calibration of Russian satellite instruments: New issues

By Rublev, A., Ju. Kiseleva, A. Uspensky, V. Golomolzin (State Research Center for Space Hydrometeorology "Planeta", Roshydromet, Moscow), D. Gayfulin and M. Tsyrulnikov (Hydrometcenter of Russia, Moscow)

According to the Russian Federal Space Program (2016–2025) the space system for hydrometeorological monitoring will consist of four LEO, three GEO and four highly elliptical orbit (HEO) satellites. Currently, two LEO (Meteor-M #2, June 2014; Meteor-M #2-2, June 2019) and two GEO (Electro-L #2 (14. 5ºW); Electro-L #3 (76ºE)) meteorological satellites are considered operational. The first satellite on HEO Arctica-M N1 was launched on February 28, 2021, and currently is undergoing the commissioning phase.

The Russian Cal/Val system designed or on-orbit calibration of meteorological satellite instruments and validation of products was developed in 2016 (GSICS Quarterly Newsletters, 2018). This paper is focused on two external calibration techniques that have been developed over past three years.

The first one is the GEO-GEO intercalibration of IR window channels of MSU-GS/ Electro-L #3 imager by using AMI/GK-2A (128ºE) and AHI/Himawari- 8 (141ºE) imagers as reference instruments.

As shown by mathematical modeling, the difference in brightness temperatures (BTs) measured by the MSU-GS and the reference instrument in window channels does not exceed 0.1 K within the calibration region (ocean waters located in the middle between two subsatellite points). Unlike the paper by Rublev et al., 2018, in which intercalibration was performed by comparing BTs measured by both instruments for the same homogeneous atmospheric scenes, another approach of GEO-GEO intercalibration has been developed.

Intercalibration is performed by equalizing the occurrence frequency histograms of TBs in MSU-GS images and similar smoothed AHI or AMI images of the calibration region. The smoothed reference images are obtained from original images in two steps. In the first step, AHI or AMI data are averaged over four pixels, taking into account that the nominal spatial resolution (2-km) of AHI and AMI imagers is twice better than the nominal spatial resolution (4-km) of MSU-GS. In the second step, the spatial Gaussian function applied as a point spread function (Khlopenkov, 2015) to averaged AHI or AMI images. The scheme for converting the AHI reference image to the MSU-GS image is shown in Figure 1. The defocusing of the reference images is carried out in accordance with the given square matrix M. Matrix elements $M_{k,n}$ are calculated by the Gaussian function $G(\sigma)$ with parameter σ:

$$M_{k,n} = G_n^k(\sigma) = \frac{1}{2\pi\cdot\sigma^2}\cdot exp\left[-\left(\frac{n^2+k^2}{2\cdot\sigma^2}\right)\right],$$

where k and n both vary from - 5 to +5.

The normalized elements of M are also used to derive the effective spatial resolution L of the MSU-GS channels.

To quantify the similarity of defocused reference images and MSU-GS ones, the number of cloud boundaries is used. The cloud boundary is determined by the threshold method applied to the BTs differences for the pair of nearby pixels

$$\left|BT_{i,j} - BT_{i+1,j}\right| > BT_h \text{ or } \left|BT_{i,j} - BT_{i,j+1}\right| > BT_h, \quad \ldots\ldots (1)$$

where a threshold BT_h= 10K; The choice of σ is based on minimizing the function

$$F(\sigma) = \sqrt{\left(\frac{NxH}{NxE} - 1\right)^2 + \left(\frac{NyH}{NyE} - 1\right)^2} = min, \quad \ldots\ldots\ldots \quad (2)$$

NxE and NyE - the normalized numbers of pair pixels for MSU-GS. where NxH and NyH - the numbers of pair pixels that meet threshold criterion (1) for the defocused image normalized to the total number of all pixels in intercalibration region; Function (2) has a single minimum and the corresponding σ specifies the effective spatial resolution L of the MSU-GS channel.

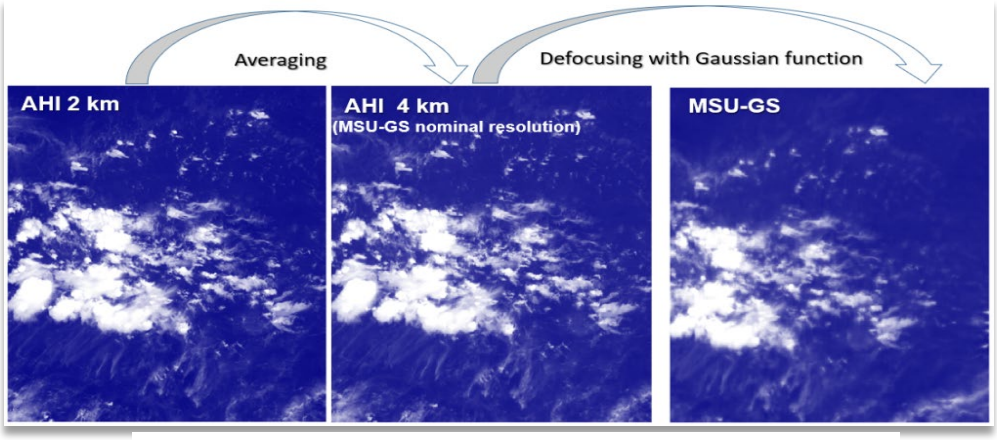

Figure 1. Scheme for processing synchronous images of two GEO imagers

doi: 10.25923/m6pq-w122

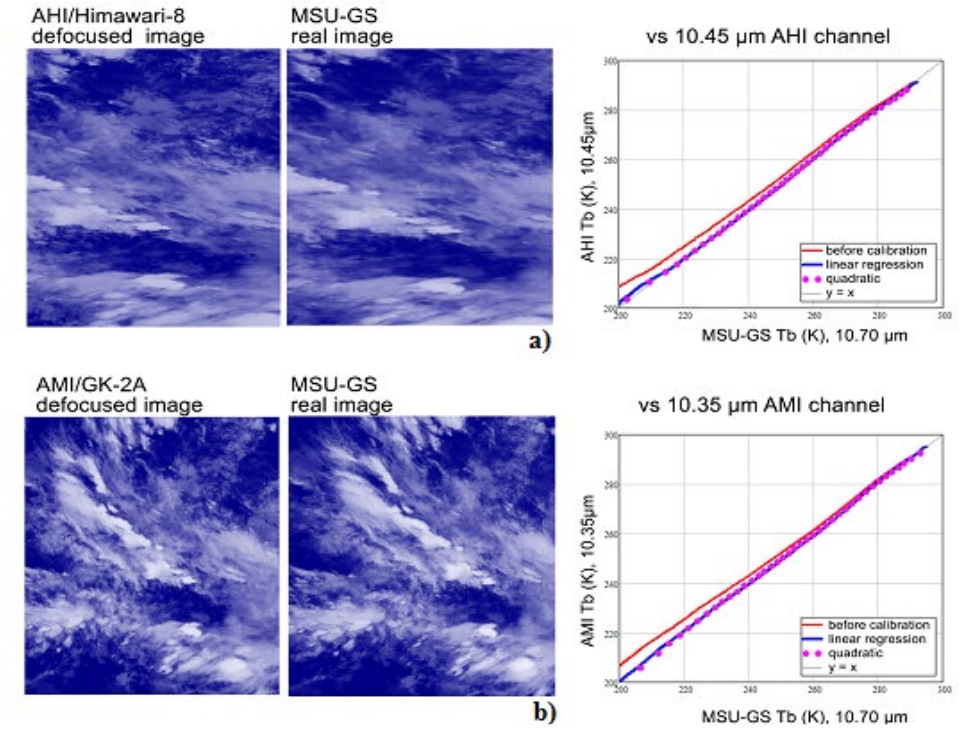

Figure 2. Intercalibration of the 9th channel MSU-GS for two ocean regions, December 12, 2020. 16:00 UTC: a) versus AHI channel; b) versus AMI channel.

As a calibration curve, a regression relationship (linear or quadratic) is used between BTs for given percentiles of their frequency of occurrence in the MSU-GS and reference defocused image.

Figure 2 shows the simultaneous images of two calibration regions MSU-GS versus AHI/Himawari-8 and AMI/GK-2A in the Pacific (a) and Indian Oceans (b) as well as the results of intercalibrations.

Note the obvious similarity of the defocused and real images obtained by reference instruments and MSU-GS for intercalibration regions. Two estimates L≈7km of real MSU-GS spatial resolution for channel #9 (σ≈0.75), reduced to the nadir direction, coincided within three hundred meters. The regression curves presented in the right part of the figure also turned out to be almost identical.

It should be emphasized that such an intercalibration allows one to estimate the possible daily variation of the calibrated instrument, and to perform this simultaneously for several GEO satellites. For example, the amplitude of the diurnal variation the MSU-GS channel #9 is 4K at BT = 220 K in respective AMI channel near 10.35 μm. At BT = 290 K, the daily amplitude does not exceed 0.4 K.

The second important issue is the on-orbit calibration of a microwave radiometer MTVZA-GYa (module for temperature and humidity sensing of the atmosphere) of LEO Meteor-M satellites (Uspensky et al., 2017). The operation of the MTVZA-GYa revealed the need to correct the measured antenna temperatures (AT) after on-board calibration when switching to the BT scale. So, an enhanced system of MTVZA-GYa measurements operational quality monitoring and control of calibration (in terms of BT) has been developed.

To determine the desired BT, the linear regression model BT = a AT + b is applied. The regression coefficients a and b are estimated using the regularized least squares method and a training sample of spatially combined and synchronous pairs (AT, reference BT). The training sample is formed for a set of pixels covering the ocean waters in the latitude zone of ±60° and filtered out atmospheric scenes with heavy clouds and precipitation. The radiative transfer model RTTOV (Saunders et al., 2018) together with the 6h GFS NCEP forecasts model as input data (with the horizontal resolution 0. 25° and the upper level of 1 hPa) is used to calculate the reference BTs. The methodology was tuned and tested on MTVZA-GYa/Meteor-M No. 2-2 data. The developed system provides online data quality control and assessment of systematic and random errors of observations, as well as bias correction by calculating and updating

Table 1. Biases and standard deviations of BTs in atmospheric sounding channels after the last on-orbit calibration (12. 02. 2021)

Channel Index	Center Frequency (GHz)& polarization	19.03.2021		24.03.2021		29.03.2021		03.04.2021		08.04.2021		14.04.2021	
		Bias	St.dev	Bias	St.dev	Bias	St.dev	Bias	St.dev	Bias	St.dev	Bias	St.dev
15	52.8V	0.18	1.41	0.21	1.42	0.09	1.37	0.03	1.41	-0.02	1.35	0.30	1.41
16	53.3V	0.16	1.07	0.25	1.04	0.11	0.97	0.03	1.01	-0.01	1.00	0.27	1.05
17	53.8V	-0.11	1.06	-0.07	1.00	-0.02	0.97	-0.09	0.96	-0.11	0.96	-0.08	1.05
18	54.64V	0.04	1.31	0.18	1.39	-0.01	1.34	-0.08	1.34	0.01	1.18	0.05	1.05
19	55.63V	0.24	1.43	0.12	1.26	0.04	1.13	-0.06	1.03	0.06	1.26	0.20	1.21
23	57±0.1H	0.11	1.17	0.18	1.17	0.01	1.15	0.00	1.12	0.03	1.24	0.12	1.12
27	183±7V	0.20	2.69	0.03	2.64	-0.28	2.61	-0.05	2.73	-0.15	2.61	0.22	2.65
28	183±3V	-0.05	2.38	-0.02	2.39	-0.16	2.31	-0.04	2.41	0.03	2.29	0.29	2.40
29	183±1.4V	-0.10	2.31	-0.15	2.33	-0.14	2.32	-0.11	2.41	-0.01	2.38	0.24	2.41

doi: 10.25923/m6pq-w122

calibration coefficients. Examples of the time behavior of biases and standard deviations are given in Table.1

The results obtained confirm that the proposed methodology allows for quality control and correction of calibration of MTVZ-GYa data in atmospheric sounding channels.

References

GSICS Quarterly Newsletter, 2018, DOI: 10. 7289/V5/QN-GSICS-12-1-2018.

Rublev, A., Gorbarenko, E., Golomolzin, V., Borisov, E., Kiseleva, Ju. , Gektin, Yu. , Zaitsev, Al. , 2018, Inter-calibration of Infrared Channels of Geostationary Meteorological Satellite Imagers. Front. Environ. Sci., 27 November 2018, 10. 3389/fenvs. 2018. 00142.

Uspensky, A., Asmus, V., Kozlov, A. et al., 2017, Absolute calibration of the MTVZA-GY microwave radiometer atmospheric sounding channels. Izv. Atmos. Ocean. Phys., Vol. 53, 1192–1204, 10. 1134/S0001433817090316

Saunders, R., Hocking, J., Turner, E. et al., 2018, An update on the RTTOV fast radiative transfer model (currently at version 12). Geosci. Model Dev., Vol. 11, Is. 7, 2717–2737, 10. 5194/gmd-11-2717-2018.

Khlopenkov, K., Doelling,D., and Okuyama A. 2015, MTSAT-1R Visible Imager Point Spread Function Correction, Part II: Theory. IEEE Transactions on Geoscience and Remote Sensing, Vol. 53, 1504-1512, No.3.

The radiometric performance of GEO-KOMPSAT-2A

By Eunkyu Kim, Minju Gu and Dohyeong Kim NMSC/KMA

The Geo-KOMPSAT-2A (hereafter GK2A, located at 128.2°E) geostationary meteorological satellite managed by the Korea Meteorological Administration (KMA) began operation at 00 UTC on 25 July 2019 (launched on 4 December 2018). The GK2A advanced Meteorological Imager (AMI) has 16 spectral channels, and its spatial resolution is 0.5 or 1 km for visible channels and 2 km for near-infrared and infrared channels.

The AMI calibration and validation methods outlined below were developed in collaboration with the KMA and the Global Space-based Inter-Calibration System (GSICS).

Visible and near-infrared channels' performance using ray matching method

GK2A AMI calibrate Visible and Near-infrared (VNIR) by using on-board absolute calibrator Solar Calibration Target (SCT) every four weeks. KMA developed various vicarious calibration methods for VNIR channels. Ray-matching is an inter-comparison method between geostationary (GEO) satellites and well-calibrated low earth orbit (LEO) satellites [1]. Selected LEO satellites are Terra MODIS (Moderate Resolution Imaging Spectroradiometer) Collection 6 and 6.1 versions from NASA (National Aeronautics and Space Administration) and Suomi-NPP (Suomi-National Polar-orbiting Partnership) VIIRS (Visible and Infrared Imager/Radiometer Suite) from NOAA (National Oceanic and Atmospheric Administration). Each 0.1° × 0.1° grid (pixels) from GEO and LEO are matched by (< ±10°) satellite and (< ±5°) solar angle, spatial resolution, and temporal interval (±5 minutes). This method has the advantage of securing data without gaps whenever LEO overpasses the GEO observation area because it does not select any specific target. Thus, it is possible to obtain the various reflectance ranges for inter-comparison. The closest matching SRFs between AMI and LEOs are used, and the SRF of LEOs are adjusted using the NASA

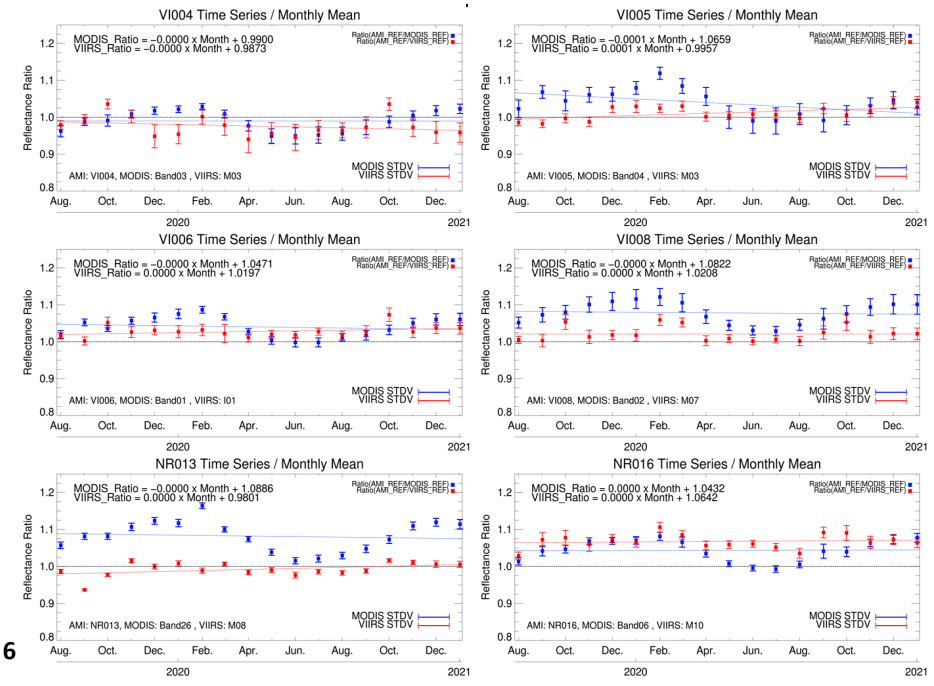

Figure 1. Ray-matching results from August 2019 to January 2021. Trends of the ratios of observation to reference computed by using the ray-matching approach. The blue squares (MODIS) and red squares (VIIRS) represent monthly averages of reflectance ratios (AMI/LEO).

doi: 10.25923/m6pq-w122

Table 1: TB mean biases and the bias at standard scene TB with respect to LEOs.

GEO LEO(K)		SW038	WV063	WV069	WV073	IR087	IR096	IR105	IR112	IR123	IR133
standard scene TB (K)		285.97	234.98	244.09	254.56	283.75	259.06	286.01	286.08	283.78	269.38
MetOp –B /IASI	bias@st	0.09	0.06	-0.12	0.01	0.02	-0.08	0.09	0.09	0.08	-0.01
	mean bias	-0.22	-0.01	-0.19	-0.03	0.12	-0.08	0.15	0.15	0.12	0.03
MetOp –C /IASI	bias@st	0.09	0.05	-0.12	0.00	0.03	-0.04	0.09	0.09	0.08	0.00
	mean bias	-0.26	-0.01	-0.19	-0.04	0.15	-0.03	0.15	0.15	0.13	0.04
NOAA20 /CrIS	bias@st	-0.01	0.05	-0.12	0.00	0.09	0.02	0.14	0.14	0.13	0.03
	mean bias	0.35	0.00	-0.18	-0.04	0.21	0.03	0.20	0.19	0.17	0.06
Suomi-NPP /CrIS	bias@st	-0.07	0.06	-0.14	-0.03	0.02	0.00	0.08	0.07	0.07	0.00
	mean bias	0.23	0.00	-0.20	-0.07	0.14	0.01	0.15	0.14	0.12	0.04

* The standard scene TB is calculated for each channel by using a radiative transfer model (RTM) based on a U.S. standard atmospheric profile and surface conditions, accounting for the SRF of each channel.

SBAF tool based on the SCanning Imaging Absorption SpectroMeter for Atmospheric CHartographY (SCIAMACHY) visible hyperspectral data [2][3].

Figure 1 shows the monthly mean reflectance ratio obtained from the ray-matching results from August 2019 to January 2021. The reflectance ratio (AMI/LEOs) was used to investigate the performance of AMI VNIR channel calibration. The reflectance ratios between AMI/MODIS show relatively large variance and strong seasonal variation compared with those between AMI/VIIRS. The magnitude of seasonal variations using the reflectance ratio (AMI/MODIS) is up to 10%, showing a minimum in summer and maximum in winter, while there is no clear seasonal variation in the reflectance ratios of AMI/VIIRS. Among the VNIR channels, the ratios between AMI and MODIS at VI004 are small (< 1.0) throughout the year except in winter, while those of the other VNIR channels are mostly ≥ 1.0.

Infrared channels' inter-calibration with Low Earth Orbit satellites

The performance of the AMI IR channel was monitored using five well-calibrated hyper-spectral sounders from LEO satellites, infrared atmospheric sounding interferometer (IASI)/MetOp-B, C and Cross-track Infrared Sounder (CrIS)/Suomi-NPP, NOAA-20 as references for inter-calibration under the framework of GSICS. AMI data from August 2019 to December 2020 were analyzed in the domain (35°N−35°S, 110°E−170°E). The target area is defined by an array of 7 × 7 AMI pixels with 2-km resolution and corresponding LEO pixel (CrIS/IASI pixel with 14 km/12 km diameters). Then, pixels with a time difference of less than 300 seconds were selected. The homogeneity of the collocation scenes is checked 21 × 21 AMI pixels centered on target area. Also, we

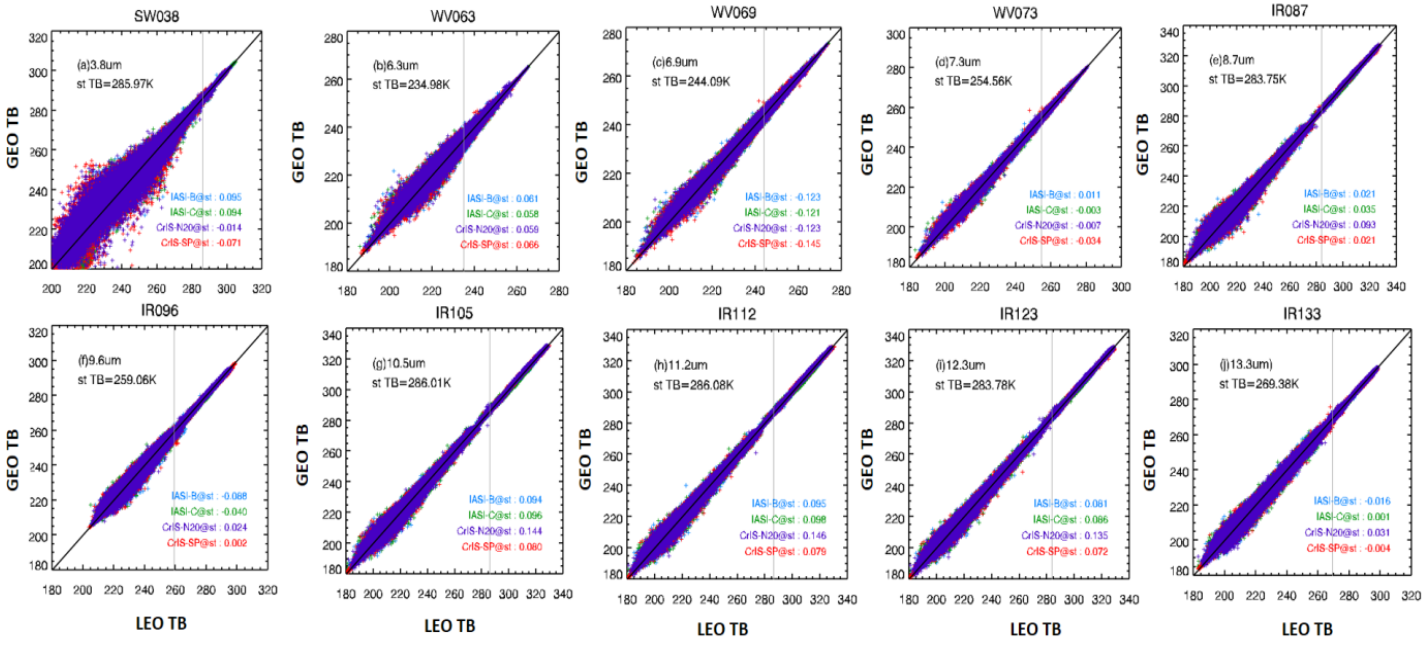

Figure 2. The scatter plot of Brightness Temperature (TB) from GK2A AMI and LEOs (IASI-B (blue), IASI-C (green), CrIS-NOAA20 (purple), and CrIS-SNPP (red)) for IR channels and grey line of standard scene TB.

doi: 10.25923/m6pq-w122

applied the normalization procedure to ensure that the radiances obtained with the different SRFs became a spectrally comparable dataset. Meanwhile, there were cases for the hyperspectral radiance of CrIS that did not fully cover the spectral bandwidth of the broadband AMI channels. So, the CrIS gap channel was provided by a gap-filling method of NOAA, which predicted the CrIS gap channels based on the principal component-based regression method [4]. In Table 1, the mean biases for TB between AMI and LEOs were within 0.21 K, except for SW038. While the biases at standard scene TB were mostly within 0.14 K. The biases are not consistent, and show slightly different values among the LEO instruments. There are relatively large biases around 0.14 K in window channels compared with CrIS of NOAA-20, while showing a large bias of -0.14 K in the upper water vapor channel with CrIS of S-NPP among the hyperspectral sounders. The largest bias at standard TB does not exceed 0.14 K among the four LEOs.

Summary

The results of radiometric calibration comparisons of GK2A AMI VNIR channels with Terra-MODIS show strong seasonal variations, whereas for NPP-VIIRS the monthly variability is small and relatively stable. Except for channel 1 (VIS048), the reflectance ratio of the other VNIR channels is greater than 1. VNIR channels' seasonal variations will be analyzed. By comparing observed collocated AMI and LEOs (IASI/MetOp-B, C, CrIS/S-NPP, NOAA-20) TB pairs for infrared channels, the biases at standard scene TB are less than 0.14 K in all infrared channels. According to GSICS results, the radiometric calibration performance of AMI infrared channels shows good stability and accuracy.

References

[1] Doelling D. R., Bhatt R., Morstad D., Scarino B., 2011. Algorithm Theoretical Basis Document (ATBD) for ray-matching technique of calibrating GEO sensors with Aqua-MODIS for GSICS, , GSICS ATBDs.

[2] Scarino, B. R., Doelling, D. R., Minnis, P., Gopalan, A., Chee, T., Bhatt, R., Lukashin, C., and Haney, C. O., 2016. A web-based tool for calculating spectral band difference adjustment factors derived from SCIAMACHY hyperspectral data, IEEE Trans. Geosci. Remote Sens., vol. 54, no. 5, pp. 2529-2542.

[3] Bovensmann, H., Burrows, J. P., Buchwitz, M., Frerick, J., Noël, S., Rozanov, V. V., Chance, K. V., and Goede, A. P. H., 1999. SCIAMACHY: Mission objectives and measurement modes, J. Atmos. Sci., vol. 56, no. 2, pp. 127-150, Jan.

[4] Xu, H., et al., 2019. Cross-track infrared sounder spectral gap filling toward improving intercalibration uncertainties. IEEE Trans. Geosci. Remote Sens., 57, 509–519

JMA 2020 GSICS Annual Report for Himawari-8/AHI

By A. Okuyama, K. Kodera, H. Tanaka, and M. Eiki (JMA/MSC)

JMA/MSC monitors the calibration performance of its Himawari-8 GEO satellite. The calibration monitoring web page was updated on 7 June. VIS/NIR band calibration performance validated via ray-matching with VIIRS was commenced in addition to the existing approach based on RTM.

On the right are the tabulated mean biases over 2020 and mean rate of calibration drift over mission lifetime.

Summary of Instrument Biases

- GSICS IR inter-calibration results are currently in the demonstration phase.

2020 Himawari-8/AHI VIS/NIR Bands Calibration Summary

AHI band name Wavelength [μm]		B01 0.47	B02 0.51	B03 0.64	B04 0.86	B05 1.6	B06 2.3	Units
Himawari-8 AHI	Mean bias (RTM)	-2.06 ± 0.33	-3.19 ± 0.29	-1.03 ± 0.28	0.03 ± 0.31	3.93 ± 0.54	-5.67 ± 0.74	%
	Annual drift (RTM)	-0.41 ± 0.04	-0.51 ± 0.04	-0.76 ± 0.04	-0.68 ± 0.04	-0.14 ± 0.05	-0.24 ± 0.05	%/yr
	Mean bias (Ray-matching)	-3.02 ± 0.54	-0.09 ± 0.66	-0.11 ± 0.66	-1.13 ± 0.70	+5.56 ± 0.90	-5.52 ± 0.74	%
	Annual drift (Ray-matching)	-0.40 ± 0.04	-0.54 ± 0.04	-0.78 ± 0.04	-0.65 ± 0.04	-0.29 ± 0.05	-0.26 ± 0.05	%/yr

* The RTM approach is based on simulation via a radiative transfer model using Aqua/MODIS. The ray-matching approach involves the utilization of SNPP/VIIRS data from the NOAA/CLASS service.

2020 Himawari-8/AHI IR Bands Calibration Summary (wrt Metop-B/IASI)

AHI band name Wavelength [μm]		B07 3.9	B08 6.2	B09 6.9	B10 7.3	B11 8.6	B12 9.6	B13 10.4	B14 11.2	B15 12.4	B16 13.3	Units
Himawari-8 AHI	Standard Radiance as Tb	286	235	244	255	284	259	286	286	284	270	K
	Mean Bias	−0.13	−0.18	−0.23	−0.14	−0.07	−0.28	+0.03	+0.03	−0.06	+0.06	K
	Std Dev	±0.01	±0.01	±0.01	±0.02	±0.01	±0.01	±0.02	±0.02	±0.02	±0.02	
	Mean Drift Rate of Bias	−0.01	−0.00	−0.00	−0.00	−0.01	−0.03	−0.01	−0.01	−0.01	−0.01	K/yr

doi: 10.25923/m6pq-w122

- There are stable biases for B05 and B06 around plus and minus 5%, respectively.

The biases for infrared bands are within ±0.3 K and are stable. The mean biases for B01, B02 and B03 in 2020 as computed using RTM are smaller than expected from the bias for 2019 and the annual drift rate. The biases for 2019 were B01: -2.01 ± 0.47; B02: -3.12 ± 0.44; B03: -0.68 ± 0.39. Biases from the ray-matching approach are within the expected range ±1-σ. Further analysis involving Solar Diffuser (SD) observation and other approaches is required. JMA/MSC monitored IR bands of AHI on Himawari-8 by comparing with IASI on Metop-A/B, AIRS on Aqua and CrIS on SNPP.

Major Calibration events in 2020

2020-07-13 Himawari-8: Update of calibration information used to correct Himawari-8 AHI sensitivity trend.

Outlook for the coming year

Himawari-8 has been stable operationally since July 2015, and the operational record is planned to be taken over by Himawari-9 in 2022.

Performance status of GSICS References IASI A/B/C

By Laura Le Barbier, Clémence Pierangelo, and Mathilde Faillot, CNES

The IASI A/B/C series of thermal infrared instruments on-board METOP(A/B/C) satellites have been designated as GSICS references for IR sensors (IASI-A up to 2019 and IASI-B since then). Indeed, IR spectrum of the IASI series spans [650 – 2760] cm^{-1} continuously and overlaps with most of the IR instruments' spectrum worldwide.

From September to November 2021, the IASI on-board METOP-A will go through end of life (EOL) campaign tests after 15 years of service, before being deorbited. These include various technological analyses, as well as providing a local improvement of spatial sampling thanks to a change in the scan pattern mode, and targeting Simultaneous Nadir Observations and Limb acquisitions during a deep space maneuver.

The IASI A/B/C global performances are monitored on a daily basis. The L0 radiometric noise is monitored once a month for each instrument thanks to the onboard blackbody views [Blumstein et al., 2004]. The fluctuations in the 700-900 cm^{-1} range is linked to the level of ice contamination (evolving more quickly during the beginning of life of each instrument). When the variation becomes important a decontamination process is planned. The plots on figure 1 show a monitoring of a year of radiometric noise in 2020 for IASI-C. The noise is similar for IASI-A and IASI-C, except that it is more stable in the 700-900 cm^{-1} range.

Every year, CNES technical expertise center performs radiometric and spectral inter-comparisons between IASI instruments using a selection of common observations (CNO) on homogenous scenes and adapting the scene selection to minimize the bias linked to geophysical conditions fast variations [Jouglet et al. 2013]. This selection process becomes more difficult with IASI-A as the METOP-A satellites orbital drift becomes important. The mean and standard deviation of the differences between two instruments for selected CNOs are computed for each channel. The method is called "Similar Bands" method (SB) as the consistency between spectral samples for both instruments is perfect and the comparison is thus rather straightforward.

The figure 2 shows that IASI-B and IASI-C instruments remain well cross-calibrated with biases ≤ 0.1K in absolute value for the whole spectral domain. The median absolute difference across all channels is 0.025K (see table 1 below).

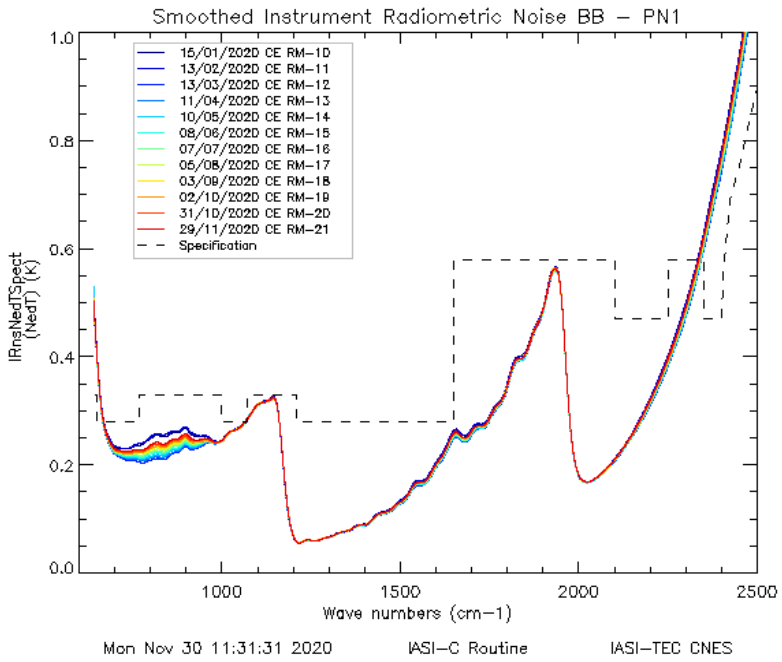

Figure 1: IASI-C radiometric noise monitoring in 2020

doi: 10.25923/m6pq-w122

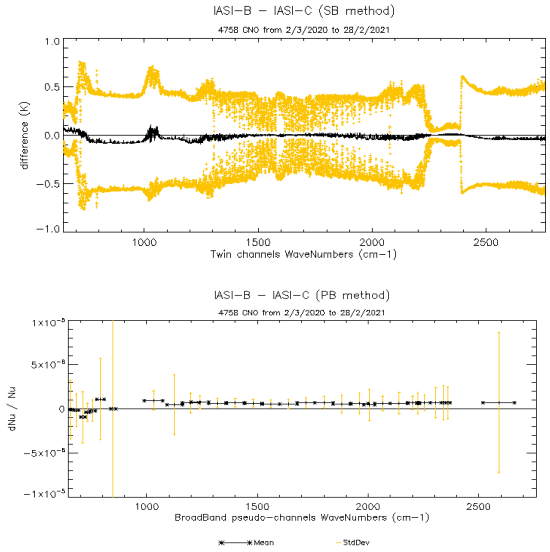

Figure 2: Upper plot: Mean (black curve) and standard deviation (yellow) of the difference IASI-B – IASI-C in brightness temperature. Lower plot: spectral inter-comparison between IASI-B and IASI-C. dNu/Nu is the relative difference in spectral calibration between IASI-B and IASI-C. 4758 CNO [March 2020 to February 2021].

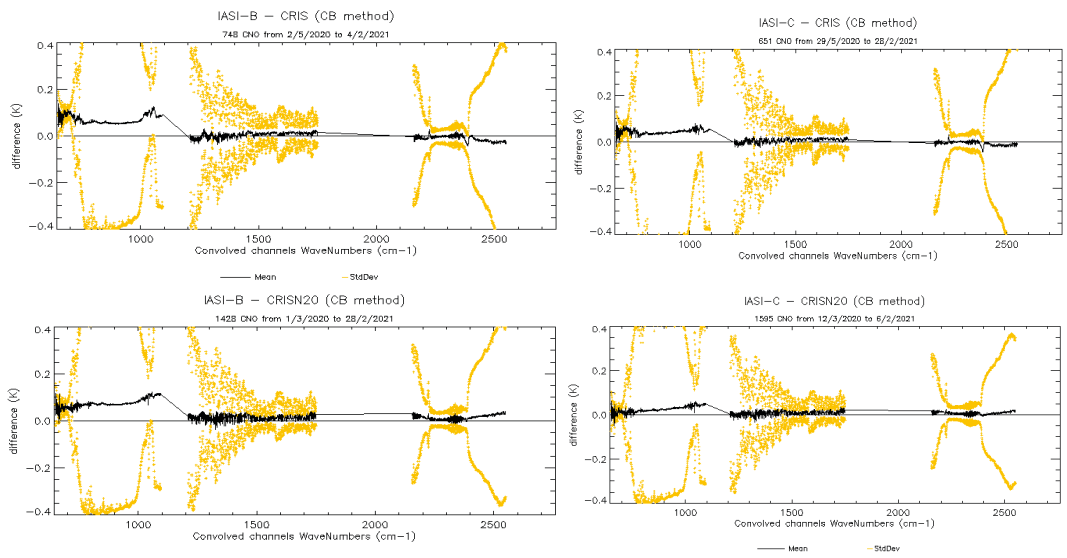

Figure 3: Mean (black curve) and standard deviation (yellow) of the difference in Brightness Temperature between: From TOP- LEFT to BOTTOM-LEFT and then TOP-RIGHT- BOTTOM-RIGT: IASI-B – CRIS/NPP (748 SNO, [May 2020 to February 2021]); IASI-B – CRIS/N20 (1428 SNO, [March 2020 to February 2021]), IASI-C – CRIS/NPP (651 SNO, [May 2020 to February 2021]); IASI-C – CRIS/N20 (1595 SNO, [March 2020 to February 2021]);

IASI-A and IASI-C instruments remain well cross-calibrated with biases ≤ 0.1K in absolute value (not shown). We now have very few CNOs (292 vs > 5000) between IASI-A and IASI-C because of IASI-A orbital drift. IASI-B and IASI-A instruments remain well cross-calibrated with biases ≤ 0.15K in absolute value (not shown). The slightly higher value can be explained by Metop-A orbital drift.

For spectral inter-calibration, the same scene selection process as the radiometric calibration is applied. Wide spectral bands with tens or hundreds of individual channels (pseudo-bands PB) are defined and the spectral analysis is performed on 30 pseudo-bands. For each pseudo-band, spectral inter-correlation is computed between the two IASI instruments in order to find the maximum of correlation which provides the spectral shift between the sensors. The relative spectral ($\Delta\nu/\nu$) shift between both sensors is plotted for each of the 30 selected pseudo-channels. For the three IASI instruments, the spectral inter-comparisons are very stable and well within the required < 2ppm. An example is provided on the lower plot of figure 2.

We also performed radiometric inter-comparisons between IASI and CRIS (CRIS/NPP at full resolution and CRIS/N20) instruments using a selection of Simultaneous Nadir observations (SNO) around the orbit crossing point and creating CRIS-like spectra from IASI spectra. As the spectral sampling and resolution of CrIS and IASI differ, the Similar Band method cannot be applied, and we use what we call the Convolution Band (CB) method. This is realized by applying a Fourier transform to IASI spectra, and dividing it by the IASI apodisation function (equivalent to a deconvolution of the spectra by IASI instrument function). Then the interferograms are resampled to the CRIS maximum optical path difference and multiplied by the CRIS apodisation function. Finally, another Fourier Transform allows us to obtain CRIS-like spectra from IASI. We obtain good cross-calibrated results, as shown in Figure 3. The median absolute value for the whole spectral domain is reported in Table 1. The difference is higher in the spectral band 1 [650 – 1210 cm^{-1}] (with maximum difference in the band between 0.06 and 0.14 K) and better for the spectral bands 2 [1210 – 1900 cm^{-1}] and 3 [1900 – 2760 cm^{-1}] (with maximum difference in the band between 0.025 and 0.045 K). Results are shown on figure 3, lower panel. The lower values are obtained for the IASI-C and CrIS/N20 differences.

Inter-comparisons are still better between IASI and CrIS than between IASI-B and IASI-C: possible reasons are linked to the orbital configuration and geophysical variations.
First, because the three IASIs are on the same orbit exactly, the inter-comparisons are performed for observations which are not simultaneous (50-minute delay)

doi: 10.25923/m6pq-w122

contrary to IASI and CrIS inter-comparisons. This could introduce systematic differences because of the diurnal cycle of thermodynamic variables. Second, when comparing spectra from two IASIs with CNO method, the observations are not nadir, because of the Earth rotation during one half-orbit, whereas IASI and CrIS inter-comparisons are nadir, which reduces the variability of the spectra.

Finally, the global repartition of observations also differs, with more polar scenes (less variable than, e.g. tropical scenes) for IASI-CrIS inter-comparisons.

In conclusion, IASI performances are still very good and stable over time. Several on-going studies will be finalized this year: the global assessment of radiometric uncertainties including non-linearity correction in the spectral band 1, the analysis of possible spectral calibration improvement and also possible cross-calibration and absolute calibration using Moon acquisitions.

Table 1: Statistics of the inter-comparisons across all the wavenumbers

	Mean	Median	Min	Max
IASI-B – IASI-C				
Bias	-0.022	-0.021	-0.094	0.104
Absolute bias	0.029	0.025		
Standard Deviation	0.40	0.45	0.04	0.76
IASI-B – CrIS/NPP				
Bias	0.022	0.009	-0.044	0.138
Absolute bias	0.031	0.016		
Standard Deviation	0.19	0.14	0.01	0.47
IASI-B – CrIS/N20				
Bias	0.034	0.022	-0.036	0.122
Absolute bias	0.035	0.022		
Standard Deviation	0.19	0.14	0.01	0.47
IASI-C – CrIS/NPP				
Bias	0.015	0.010	-0.043	0.086
Absolute bias	0.021	0.013		
Standard Deviation	0.20	0.14	0.01	0.50
IASI-C – CrIS/N20				
Bias	0.014	0.012	-0.050	0.063
Absolute bias	0.015	0.013		
Standard Deviation	0.17	0.13	0.01	0.42

References:

Blumstein, D., Chalon, G., Carlier, T., et al., "IASI instrument: technical overview and measured performances," Proc. SPIE 5543, Infrared Spaceborne Remote Sensing XII, (4 November 2004); doi: 10.1117/12.560907

Jouglet, D., Chinaud, J., Lenot, X., Radiometric inter-comparison of IASI: IASI-A / IASI-B, IASI / AIRS, IASI / CrIS, 3rd IASI conference, 4-8 February 2013, Hyères, France

Vis/NIR subgroup proposes TSIS-1 HSRS as the GSICS recommended solar spectrum

By Thomas C. Stone, USGS, Odele Coddington, LASP, Juseon Bak, PNU-IES (Pusan National University, Institute of Environmental Studies), Dave Doelling, NASA-LaRC

The solar spectral irradiance (SSI) is a fundamental component of reflectance calibrations for visible to shortwave infrared (VSWIR) sensors. In recent years, the solar reference spectrum of Thuillier et al. [1] has been used extensively. However, calibration of spectrally resolved sensors such as hyperspectral imagers require higher spectral resolution for the reference solar spectrum. At the 2019 GSICS annual meeting in Frascati, a

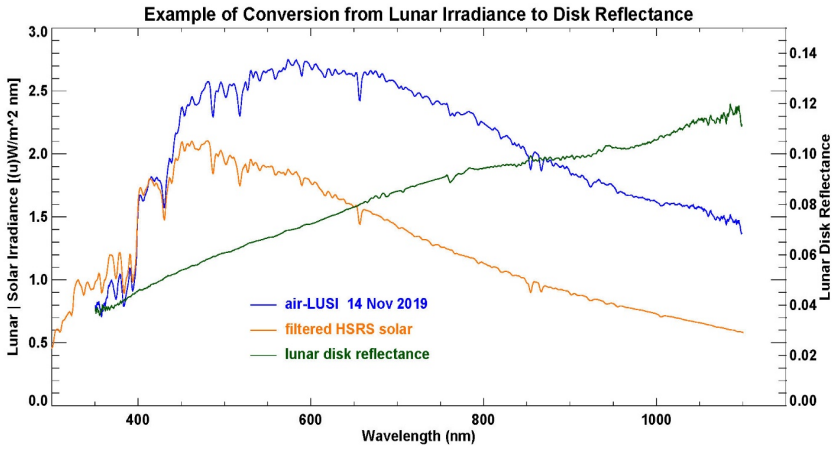

Figure 1. Example of conversion from lunar spectral irradiance (blue) to disk reflectance (green) using a filtered solar spectrum (orange). The filtered TSIS-1 HSRS accurately aligns with the air-LUSI measurement to offset the Fraunhofer structure and produces a smooth reflectance spectrum.

doi: 10.25923/m6pq-w122

presentation to the Vis/NIR subgroup given by Dr. Odele Coddington of the Laboratory for Atmospheric and Space Physics (LASP) described the then-new TSIS-1 SSI and total solar irradiance measurements. The ensuing discussion identified the need for a static solar spectrum having both high accuracy and high spectral resolution. Accommodating these two priorities simultaneously requires merging solar datasets.

LASP agreed to undertake this task and produced the TSIS-1 Hybrid Solar Reference Spectrum (HSRS), spanning 202 nm to 2730 nm with 0.01 to 0.001 nm spectral resolution and 0.3% to 1.3% uncertainty. The TSIS-1 HSRS was constructed by adjusting high spectral resolution solar line datasets to the high-accuracy, but lower spectral resolution, TSIS-1 SIM and Compact SIM (CSIM) SSI observations [2]. TSIS-1 SIM and CSIM observe SSI at higher accuracy than attained by predecessor instruments and, notably, show the near-infrared solar spectrum is up to 8-10% lower in magnitude than other reference spectra including Thuillier et al. [1]. The TSIS-1 HSRS uncertainty encapsulates the uncertainty in the TSIS-1 and CSIM SSI observations and the accuracy to which the high-resolution solar line data can be adjusted to the TSIS-1 and CSIM SSI scale. Variants of the TSIS-1 HSRS with fixed spectral resolution of 0.005 nm, 0.025 nm, 0.1 nm, and 1 nm were also produced. The URL link for access is: https://lasp.colorado.edu/lisird/data/tsis1_hsrs

The high spectral resolution solar line datasets that are adjusted to the TSIS-1 and CSIM SSI irradiance scales using a modified spectral ratio method include: the Airforce Geophysical Laboratory (AFL) solar irradiance balloon observations from 200-310 nm at 0.01 nm resolution; ground-based solar irradiance observations spanning 305 nm to 380 nm at 0.025 nm resolution from the Quality Assurance of Ultraviolet Measurements In Europe (QASUMEFTS) campaign; the Kitt Peak National Observatory (KPNO) solar transmittance atlas developed from ground-based observations spanning 300 nm to 1000 nm at ~0.001 nm spectral resolution; the Solar Pseudo-Transmittance Spectrum (SPTS) atlas containing 40,000 solar absorption lines spanning 380 nm to 16,600 nm at ~0.001 nm spectral resolution.

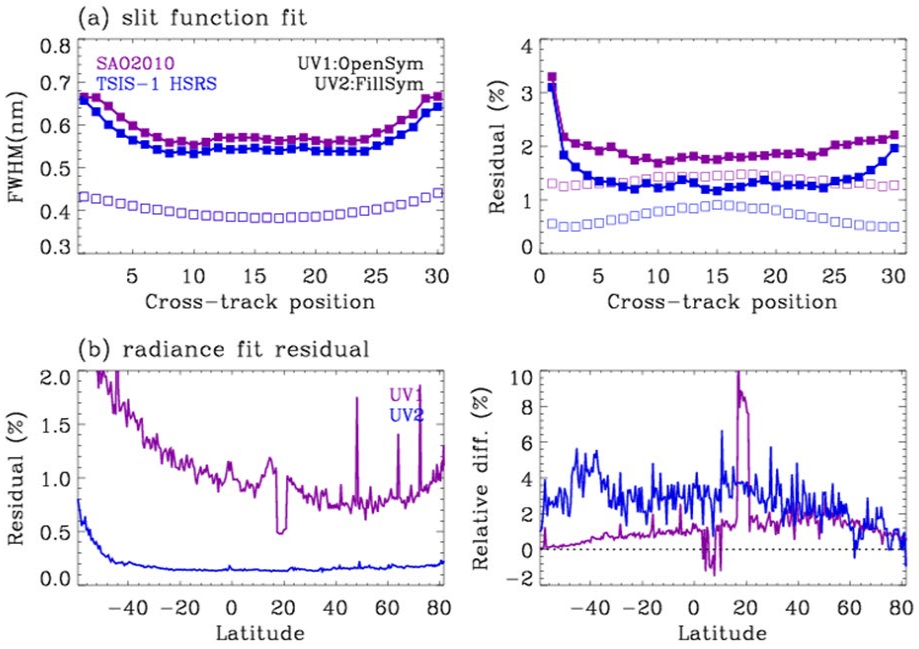

Figure 2. (a) Comparison of fitting slit widths from OMI irradiances for UV1 (270-310 nm) and UV2 (310-330 nm) ranges, and fit residuals. Slit widths are fitted as a Full width at Half Maximum (FWHM) of a Gaussian function. Residuals are calculated as $\sqrt{\frac{1}{N}\sum\left|\frac{I_{OMI}-I_{SIM}}{I_{OMI}}\right|^2} \times 100$ (%) where I_{OMI}/I_{SIM} is measured/simulated spectrum. (b) Results for performing ozone retrievals from OMI radiance measurements. In left panel, the evaluated variables are derived when using TSIS-1 HSRS; the right panel shows relative difference as: (SAO2010 – TSIS-1 HSRS) / SAO2010.

The TSIS-1 HSRS encompasses an integrated energy in excess of 97% of the total solar irradiance. This provides an important new constraint of the solar irradiance spectrum for science analysis in a broad array of fields.

A recent application of the TSIS-1 HSRS involved observations acquired by the airborne Lunar Spectral Irradiance (air-LUSI) instrument aboard the NASA ER-2 high-altitude aircraft. The analysis converted the air-LUSI irradiance measurements to disk reflectance by dividing out the solar spectrum, as shown in Fig. 1. This requires a solar spectrum that has been filtered to the wavelength grid and spectral response line shapes of the air-LUSI spectrograph, which in turn requires a reference solar spectrum with higher resolution than the instrument. The success of this process is clear in the figure, where the complex Fraunhofer structure is accurately aligned in wavelength and strength to offset the measurement, giving a smooth reflectance spectrum that is expected for the Moon.

In another recent application, Dr. Juseon Bak investigated the impact of switching the solar reference from SAO2010 [3] to TSIS-1 HSRS on ozone profile retrievals from the Ozone

Monitoring Instrument (OMI). For these retrievals, an optimal estimation-based inversion is applied to OMI measurements in the spectral range 270-330 nm [4]. A well-calibrated high resolution solar spectral irradiance is important for characterizing wavelength assignment and slit functions by means of matching the solar Fraunhofer absorption lines between measured and reference spectra, as well as for the convolution process in forward model simulation. In fitting OMI slit shapes as a Gaussian, derived slit widths differ by 0.02 nm due to different solar reference datasets, with fitting uncertainties being smaller (by 0.5%) when TSIS-1 HSRS is used as a reference to OMI irradiances (Fig.2a). In performing ozone retrievals from OMI earthshine measurements, fitting residuals decrease by up to 2% in the UV1 range as well as by ~5% in the UV2 using TSIS-1 HSRS (Fig 2b).

Reflective solar band imagers that utilize onboard solar diffusers rely on a reference solar spectrum for deriving L1B radiance products from calibrated reflectance measurements. For example, the VIIRS imagers onboard the SNPP and NOAA-20 platforms use the Kurucz spectra from MODTRAN 4.0 and Thuillier 2003 solar spectra, respectively. The corresponding band radiances between the two VIIRS sensors can differ by up to 3% due to the solar spectra implemented, even if both sensors' reflectance measurements were perfectly inter-calibrated [5]. To eliminate the need for individually computing reflectance and radiance-based inter-calibration ratios, a common recommended solar spectrum should be used across the satellite data products. The importance of documenting the solar spectra utilized in satellite data products cannot be overstated. Lastly, the upcoming CLARREO Pathfinder mission will incorporate the HSRS solar spectra to provide radiances from the observed SI traceable reflectances.

The high accuracy demonstrated by the TSIS-1 HSRS is expected to lead to its widespread adoption for Earth observing sensor calibration applications, supplanting the commonly used Thuillier spectrum. Recognizing the recent successful applications, the Vis/NIR subgroup has proposed recommending the TSIS-1 HSRS for GSICS applications and promoting this recommendation to the wider community. A first step is to coordinate with the CEOS-IVOS group.

References

1. Thuillier, G. *et al.* (2003) The Solar Spectral Irradiance from 200 to 2400 nm as Measured by the SOLSPEC Spectrometer from the Atlas and Eureca Missions. *Solar Physics* **214,** 1–22. https://doi.org/10.1023/A:1024048429145

2. Coddington, O. M., Richard, E. C., Harber, D., Pilewskie, P., Woods, T. N., Chance, K., et al. (2021). The TSIS-1 hybrid solar reference spectrum. *Geophysical Research Letters*, **48**, e2020GL091709. https://doi.org/10.1029/2020GL091709

3. Chance, K. and Kurucz, R. (2010), An improved high-resolution solar reference spectrum for Earth's atmosphere measurements in the ultraviolet, visible, and near infrared, *J. Quant. Spectrosc. Rad. Trans*., **111**, 1289–1295. https://doi.org/10.1016/j.jqsrt.2010.01.036.

4. Liu, X., Bhartia, P.K, Chance, K, Spurr, R.J.D., and Kurosu, T.P. (2010), Ozone profile retrievals from the ozone monitoring instrument. *Atmos. Chem. Phys*., **10**, 2521–2537. https://acp.copernicus.org/articles/10/2521/2010/

5. Bhatt, R.; Doelling, D.R.; Coddington, O.; Scarino, B.; Gopalan, A.; Haney, C. (2021) Quantifying the Impact of Solar Spectra on the Inter-Calibration of Satellite Instruments. *Remote Sens*., **13**, 1438. https://doi.org/10.3390/rs13081438

NEWS IN THIS QUARTER

Highlights of the 2021 Annual GRWG/GDWG Meeting

By M. Bali (UMD), L. Flynn (NOAA), S. Hu (CMA), T. Stone (USGS), D. Doelling (NASA), Quanhua (Mark) Liu (NOAA), T. Hewison (EUMETSAT), F. Yu (NOAA), L. Wang (NOAA) and D. Kim (KMA)

This year's meeting of the GSICS Research and Data Working Groups (GRWG and GDWG) was hosted virtually by NOAA 29 March –2 April 2021. Members from ACRI, CMA, CAS, CNES, ECMWF, EUMETSAT, ESA, ISRO, JAXA, JMA, KMA, LASP, NIST, NASA, NOAA, NPL, RAL, Rayference, ROSHYDROMET, ROSCOSMOS, UKMO, USGS, VITO and WMO attended the meeting. Larry Flynn (GCC Director) opened the meeting and welcomed the participants.

doi: 10.25923/m6pq-w122

Plenary Day-1

The first session of the meeting was a Plenary which spread across the first two days of the meeting. The first day of the Plenary was chaired by Xiuqing Hu (CMA) and covered topics vital to GSICS in the near future. Reprocessing was one of the themes of the Plenary reports this year.

The first day had presentations and discussions on GSICS –CEOS interaction (led by Akihiko Kuze Chair CEOS) and GSICS –ISCCP interactions (led by Andy Heidinger, NOAA). Andy reported on the plans to develop cloud climatologies from GSICS corrections over the GEO-Ring and provided recommendations to GSICS on tuning their products to fulfill needs of the ISCCP community. Both the talks (CEOS and ISCCP) focused on strengthening the GSICS bond with users of its algorithms, deliverables and products. Talks by personnel from ESA, KMA, IMD and CMA, covered important advances they made in developing satellite monitoring strategies and sharing knowledge. CMA showed the benefits of using GSICS corrections and their focus in reprocessing and developing climate data records. Philippe Goryl (ESA) mentioned that ESA calibration landing page have been updated on the WMO/OSCAR and commented on ESA's contributions to the special issue of the GSICS newsletter on Sentinel-2. Further, ESA's contribution to Lunar activities (LIME), TRUTHS Mission and the Tandem project can greatly aid in taking GSICS activities forward. On the reprocessing front, ESA has a comprehensive program (including FDR4ATMOS and FDR4ALT) that target instruments such as SCIAMACHY, ERS-2GOME and ENVISAT (A/ATSR), Sentinel-3, and Cryosat.

The Data Working Group report was provided by Manik Bali (UMD). He reported that the GDWG now has a new chair (Kamaljit Ray, IMD), and among the new tools developed by the GDWG to support GRWG activities are the following: Github (KMA), GSICS Product Status System (NOAA), Collaboration Server (EUMETSAT), EVDC (ESA) and Google Colab Notebooks (NOAA). He encouraged members to use try the tools and report on any issues.

CNES provided the status of the performance matrix of the IASI-A/B/C instrument and provided a timeline of the IASI-A decommissioning process. IASI-B/C continue to provide reference measurements and their records are available for use as GSICS references.

Plenary Day-2

The second day of the Plenary was chaired by Fangfang Yu (NOAA) and had presentations from EUMETSAT, JAXA, JMA, ROSHYDRO, NIST, NASA and NOAA.

Misako Kachi (JAXA) provided a summary of JAXA activities which included inter-calibration of GCOM-C/SGLI by GIRO. She mentioned that JAXA has completed the reprocessing of AMSR-E, GOSAT and GOSAT-2.

Arata Okuyama (JMA) provided details of GSICS correction products (H-8 and MTSAT-2) and mentioned that JMA is working on gap filling algorithms.

Pradeep Thapliyal (ISRO) relayed advances in acquiring IASI data for intercalibration and the status of GSICS style monitoring of INSAT-3D/3DR.

Tim Hewison (EUMETSAT) reported that they are moving to second generation of MetOp and third generation Meteosat. Tim provided a summary of GSICS products. Upcoming activities included DCC Calibration and FCDR generation. Tim also engaged the GSICS community by sharing with them the feedback that he received from the NWP community on Radiometric and Spectral Biases. It was decided to invite NWP community to GSICS meetings.

Next, Viju John (EUMETSAT) provided details about EUMETSAT FCDR generation (reprocessing) activities.

Alexey Rublev (ROSHYDROMET) provided the status of satellites and provided a report on intercalibration of Meteor with Korean Satellites.

Xianqian Wu (NOAA) provided a detailed overview of instrument monitoring (GOES-16/17) and the health of GSICS references (VIIRS and CrIS). He also mentioned new GOES ABI vs. CrIS/IASI products generated by NOAA and submitted to the GPPA.

Jack Xiong (NASA) provided details on improvements made in S-NPP, NOAA-20 and JPSS-2/3, Landsat 8/9. Jack also mentioned NASA collaborations with the SmallSat community.

Stephen Maxwell (NIST) provided updates on NIST contributions to GSICS activities. This mainly focuses on Lunar Calibration (MLO-LUSI), MOBY and VACNT.

UVNS Spectrometer Sub-Group

There were over 50 participants for the UVNS Spectrometer Subgroup Session. Ten talks were presented by researchers from eight agencies with eight talks covering the calibration and validation of Level 1 radiance and irradiance measurements from GK-2B GEMS, FY3 OMS, GF-5/EMI, S5p TropoMI, Metop-A/B/C GOME-2, EOS Aura OMI, NPP/N20 OMPS, OCO-2 and ISS OCO-3, and two talks describing the inter-instrument adjustments used in the development of Climate Data Records from GOME, SCIAMACHY, SBUV(/2) and OMPS. The GEMS instrument is operating in a GEO orbit and provides new opportunities for

doi: 10.25923/m6pq-w122

GEO/LEO comparisons for LEO UV and Visible spectrometers.

IR Sub-Group

The IR group covered the inter-calibration of IR bands in narrow- and broad-band instruments and hyperspectral IR sounders through direct or indirect (double difference) comparison using NWP RTM simulations, Ground based measurements, and other observations. In lieu of the 2021 GSICS annual meeting, the IR group hosted two sessions. The first one was held on April 1 2021 and focused on general topics on IR calibration as well as the calibration of hyperspectral IR sounders. The second on was held on April 8 2021and included reports on the status of the GEO-LEO IR products from NOAA, CMA, JMA, EUMETSAT.

Overall, the reference instruments, CrIS and IASI, are very stable. One of the main thrusts has been to connect with the ISCCP and NWP community. The team continues to work on the PCA based gap filling method by further extending IASI shortwave spectra and covering more channels. An investigation of IASI -inter-calibration bias at SW (3.9 Micron) was found to be due to the incorrect handling of negative radiances. Efforts have been made to improve GEO-GEO and GEO-LEO inter-calibration algorithms.

The Subgroup needs a new chair – nominations will be accepted. In the future, we have to plan more meetings, support more cross-community efforts (ISCCP, WGCV), expand membership and share tools using github and the GSICS wiki.

MW Subgroup

The GSICS GRWG Microwave Subgroup (MWSG) breakout meeting reflected the Subgroup's diverse agenda over the past year. The meeting included presentations providing information on microwave instrument status, application of microwave data and GSICS products to NWP and reanalysis projects, FCDR development, calibration assessment method application, and SI traceability in microwave remote sensing. A briefing and ensuing discussion also focused on the MWSG progress in the past year and its way forward.

During the meeting, many important points were voiced. The group was encouraged to be more active in working towards producing inter-calibration products to improve the inter-operability of current microwave instruments. GPM X-Cal has been a start. Also, GSICS-related applications of lunar calibration and Simultaneous Nadir Overpass (SNO) and observed (O) minus background (B) simulated brightness temperature inter-calibration methods were presented but have not been formalized into GSICS products. The possibility of CubeSat and SmallSat microwave instrument constellations will increasingly require well documented inter-calibration methods to make the data more readily usable. Regarding new MW instrument generations, the possible effect of 5G telecommunications on radiometer signals is a MWSG concern, and JAXA revealed a workaround for the upcoming AMSR3 instrument. GSICS outreach to the NWP community took a spotlight in the meeting, with a budding collaboration developing to utilize NOAA ATMS data reprocessing in ERA-5 reanalysis. Collaboration amongst agencies within GSICS were evident during FCDR discussions, as there is a desire to use FIDUCEO-determined uncertainties to improve communication of FCDR skill. Finally, basic SI traceability concepts were introduced, and information was proffered about the type of microwave measurements that exist and to which SI standards they are traceable to.

VIS/NIR Sub-Group

One of the key activities over the past year has been to arrive at a reference solar. Odele Coddington (LASP) recommends the TSIS-HSRS dataset as the GSICS VIS/NIR reference solar spectra. (See the preceding article for details.) CLARREO PF (ISS 2023) and TRUTHS on orbit VIS/NIR traceable sensors will soon provide absolute calibration references.

Among key achievements is that Raj Bhat has come up with a new DCC calibration method needed for next generation GEO imagers. It uses a DCC PDF inflection point which shows stability in sparse sampling. The N20 VIIRS is the next GSICS recommended on-orbit calibration reference for Vis/NIR bands. Since differences between the two N20-VIIRS SDRs are small, either can be used as a reference.

Tom Stone (USGS) briefed on results for the Lunar area of Vis/NIR work. This included the Lunar workshop, and Lunar Model inter-comparison exercises, and more development on LIME and LESSSR. The GSICS Vis/NIR sub-group will have monthly meetings during the coming year.

GSICS Data Working Group

The GDWG session started with a review of the status of GDWG actions. ESA kindly gave three talks relevant to their data management activities. All the presentations were highly appreciated by the group, and further collaboration such as a nomination of ESA GDWG member and close communication with CEOS/WGISS were discussed. The group also welcomed an active involvement of ROSHYDROMET, who launched their GSICS website and Landing Page for satellite and instrument Event Logging. Issues on the Event Logging such as an

doi: 10.25923/m6pq-w122

entity maintaining the pages and a way to achieve the goal to adopt nomenclature and data standards were raised, and will be discussed further with the GSICS-EP. One of the most important collaboration activities for GDWG is the GSICS Collaboration Servers, which provide a set of services to support data exchange and access to relevant inter-calibration datasets. In addition to the current servers operated by CMA, EUMETSAT and NOAA, ISRO reported their progress on building a THREDDS server which is expected to be fourth Collaboration Server. The collaborative work among the member agencies for updating server configuration and data synchronization are ongoing. A need for adding a new value (SRF) to the Common Table C-13 of WMO Manual on Codes was raised to satisfy the GSICS Convention for Spectral Response Function files. The group agreed the needs and is further presented to EP for their endorsement. CMA's proposal to share Level 1 subsets over PICS and SNO Prediction could be useful for GRWG activities, so it was agreed to be reported to GRWG. The group also agreed to continue other collaborative activities such as GSICS Product download scripts, Quicklooks on Product Catalog, the GSICS Plotting Tool and the Action Tracking Tool.

Cross cutting discussions

The concluding day of the meeting was chaired by Larry Flynn (GCC Director / NOAA). This session held cross cutting discussions, attempted to summarize the discussions members had during the week of the Annual meeting and reviewed Actions, Decisions and Recommendations generated during the meeting. The session also discussed future hosting of the GSICS Annual Meetings.

As part of this session, GRWG, GDWG groups and subgroups, GIR, GMW, GUV and GVIS/NIR presented overviews of discussions they had in the breakout sessions, and the GCC report was presented by Larry, and indicated the growing trend in GSICS memberships and gave an update on the new products accepted into the GSICS product catalog.

Mitch Goldberg (GSICS EP Chair) discussed the GSICS State of the Observing System report and the status of the Special Issue of the GSICS Newsletter on State of Observing System.

Members agreed that despite being hit by the COVID crisis, GSICS member agencies maintained steady progress in GSICS activities. Member agencies reporting on results of re-processing activities demonstrated the benefits of using GSICS cross calibration in reducing biases and variance in satellite measurements. Members also agreed to increase the frequency GSICS web meetings to once a month for most GRWG Sub-groups.

Chairs reported that most of the actions were closed and new actions were extracted from the discussions that would pave the way for future development of GSICS algorithms, data and collaboration.

The meeting agenda and presentations are on the GSICS wiki page http://gsics.atmos.umd.edu/bin/view/Development/Annual2021
Actions, Recommendations & Decisions will be published on the GCC website.

doi: 10.25923/m6pq-w122

Announcements

CEOS WGCV-49 Meeting to be held June 29 - July 2, 2021

By Akihiko Kuze, JAXA

The 49th Meeting of the CEOS Working Group on Calibration and Validation would be virtual meeting.
This will be a 4-day meeting of two hours each day, starting on June 29, 2021. The starting time will be 12:00 UTC (08:00 Washington DC, 13:00 London, 14:00 Rome, 20:00 Perth, 21:00 Tokyo) each day. Details are on https://ceos.org/meetings/wgcv-49/

GSICS-Related Publications

Alexanin, A.I., and S.E. Diakov. 'IR Channels Calibration of the MSU-MR Radiometer of the Meteor-M No. 2-2 Satellite [Калибровка ИК-Каналов Радиометра МСУ-МР Спутника «Метеор-М» № 2-2]'. *Sovremennye Problemy Distantsionnogo Zondirovaniya Zemli Iz Kosmosa* 18, no. 1 (2021): 70–77. https://doi.org/10.21046/2070-7401-2021-18-1-70-77.

Bhatt, R., D.R. Doelling, O. Coddington, B. Scarino, A. Gopalan, and C. Haney.'Quantifying the Impact of Solar Spectra on the Inter-Calibration of Satellite Instruments'. *Remote Sensing* 13, no. 8 (2021). https://doi.org/10.3390/rs13081438.

Chaity, Manisha Das, Morakot Kaewmanee, Larry Leigh, and Cibele Teixeira Pinto.'Hyperspectral Empirical Absolute Calibration Model Using Libya 4 Pseudo Invariant Calibration Site'. *REMOTE SENSING* 13, no. 8 (April 2021). https://doi.org/10.3390/rs13081538.

Jin, D., Lee, S., Lee, S., Jung, D., Sim, S., Huh, M., & Han, K. (2021). Evaluation of GSICS Correction for COMS/MI Visible Channel Using S-NPP/VIIRS. 대한원격탐사학회지, *37*(1), 169–176. https://doi.org/10.7780/KJRS.2021.37.1.14

Kim, D., M. Gu, T.-H. Oh, E.-K. Kim, and H.-J. Yang. 2021. 'Introduction of the Advanced Meteorological Imager of Geo-Kompsat-2a: In-Orbit Tests and Performance Validation'. *Remote Sensing* 13 (7). https://doi.org/10.3390/rs13071303.

Khakurel, P., L. Leigh, M. Kaewmanee, and C.T. Pinto. 'Extended Pseudo Invariant Site-Based Trend-to-Trend Cross-Calibration of Optical Satellite Sensors'. *Remote Sensing* 13, no. 8 (2021). https://doi.org/10.3390/rs13081545

Liu, Li, Tingting Shi, Hailiang Gao, Xuewen Zhang, Qijin Han, and Xinkai Hu. 'Long-Term Cross Calibration of HJ-1A CCD1 and Terra MODIS Reflective Solar Bands'. *Scientific Reports* 11, no. 1 (1 April 2021): 7386. https://doi.org/10.1038/s41598-021-86619-y

MJ Burgdorf, SA Buehler, M Prange, 2021, Calibration and Characterisation of Satellite-Borne Microwave Sounders With the Moon, doi: https://doi.org/10.1029/2021EA001725

Saunders, R. W., T. A. Blackmore, B. Candy, P. N. Francis and T. J. Hewison, "Ten Years of Satellite Infrared Radiance Monitoring With the Met Office NWP Model," in *IEEE Transactions on Geoscience and Remote Sensing*, vol. 59, no. 6, pp. 4561-4569, June 2021, doi: https://doi.org/10.1109/TGRS.2020.3015257.

Zhipeng Wang, Xiangqian Wu, Fangfang Yu, Jon P. Fulbright, Elizabeth Kline, Hyelim Yoo, Timothy J. Schmit, Mathew M. Gunshor, Monica Coakley, Mason Black, Daniel T. Lindsey, Haifeng Qian, Xi Shao, and Robbie Iacovazzi "On-orbit calibration and characterization of GOES-17 ABI IR bands under dynamic thermal condition," Journal of Applied Remote Sensing 14(3), 034527 (30 September 2020). https://doi.org/10.1117/1.JRS.14.034527

doi: 10.25923/m6pq-w122

Submitting Articles to the GSICS Quarterly Newsletter:

The GSICS Quarterly Press Crew is looking for short articles (800 to 900 words with one or two key, simple illustrations), especially related to calibration / validation capabilities and how they have been used to positively impact weather and climate products. Unsolicited articles may be submitted for consideration anytime, and if accepted, will be published in the next available newsletter issue after approval / editing. Please send articles to manik.bali@noaa.gov.

With Help from our friends:

The GSICS Quarterly Editor would like to thank Tim Hewison (EUMETSAT), Dave Doelling (NASA), Fangfang Yu (NOAA) and Lawrence Flynn (NOAA) for reviewing articles in this issue. Thanks are due to Jan Thomas (NOAA) for helping with 508 compliance.

Published By

GSICS Coordination Center
NOAA/NESDIS/STAR NOAA
Center for Weather and Climate Prediction,
5830 University Research Court
College Park, MD 20740, USA

CISESS
5825 University Research Court, Suite 4001,
University of Maryland, College Park, MD 20740-3823